catalysts

MDPI

Article

Catalytic Degradation of Organic Contaminants by Microwave-Assisted Persulfate Activation System: Performance and Mechanism

Yunhe Li [1], Weibao Liu [1], Lezhuo Li [2,*], Siyuan Jiang [1] and Xiuwen Cheng [1,2,*]

[1] Key Laboratory for Environmental Pollution Prediction and Control, Gansu Province, College of Earth and Environmental Sciences, Lanzhou University, Lanzhou 730000, China
[2] Engineering Research Center for Cold and Arid Regions Water Resource Comprehensive Utilization (Ministry of Education), School of Environmental and Municipal Engineering, Lanzhou Jiaotong University, Lanzhou 730070, China
* Correspondence: lilezhuo@163.com (L.L.); chengxw@lzu.edu.cn (X.C.)

Abstract: In this study, a nickel ferrite ($NiFe_2O_4$) system was constructed to purify a phenol solution in water. During the process, the influences of several critical operating parameters including the $NiFe_2O_4$ amount, PS dosage, MW power, initial pH value, and different natural water anions were systematically studied. The results indicated that the constructed system performed excellently regarding the removal efficiency (97.74%) of phenol within 30 min. Meanwhile, the influence of co-existing anions such as Cl^-, NO_3^-, $H_2PO_4^-$, and HCO_3^- was also studied, which displayed an inhibiting action on phenol degradation, while HA facilitated it. To explore the reaction mechanism of this system, major free radical quenching experiments were conducted, and it was confirmed that both $SO_4\bullet^-$ and HO• were primary radicals. Moreover, stability experiments confirmed the apt stability of the $NiFe_2O_4$ system. Besides, the mineralization and toxicity analysis performed during phenol degradation also confirmed the superiority of the as-constructed system. Furthermore, the possible degradation mechanism of phenol was proposed. Hence, this system could be applied in advanced wastewater treatment.

Keywords: persulfate; microwave; sulfate radicals; phenol; nickel ferrite

Citation: Li, Y.; Liu, W.; Li, L.; Jiang, S.; Cheng, X. Catalytic Degradation of Organic Contaminants by Microwave-Assisted Persulfate Activation System: Performance and Mechanism. *Catalysts* **2022**, *12*, 1232. https://doi.org/10.3390/catal12101232

Academic Editors: Jiangkun Du, Lie Yang and Chengdu Qi

Received: 9 September 2022
Accepted: 9 October 2022
Published: 14 October 2022

1. Introduction

People are increasingly concerned about environmental pollution caused by recalcitrant organic contaminants such as antibiotics, pesticides, surfactants, dyes, and hydrocarbons, which may include phenols, ammonia, cyanides, sulfides, and aromatic compounds [1–3]. Most phenols and their derivatives are persistent organic pollutants and may harm organisms even in low doses [3,4]. Therefore, attention has been increasingly paid to phenolic wastewater treatment [5]. PS can be seen as the product of the substitution of two hydrogen atoms in H_2O_2 by sulfonyl-SO_3H. It is a white crystal and is very soluble in water. Figure 1 shows the PS structure.

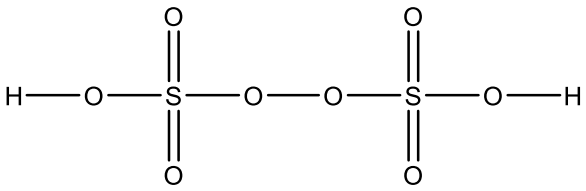

Figure 1. PS structural formula.

Microwaves (MWs) activate PS to degrade organics by different mechanisms. In this process, in addition to the widely accepted thermal effect, the specific effect also plays

an important role [3,6,7]. This feature could reduce the number of intermediate products from organic matter degradation and is conducive to the removal of refractory organic matter [8,9]. Compared with traditional heating methods, the MW thermal effect has the superiority of no heat transfer process demands, simultaneous heating of the whole system, outstanding heating uniformity, and no secondary pollution [10,11]. Moreover, MW could create more micropores on the surface of the material, thus improving the adsorption and PS activation properties of the material [12,13]. For instance, a significant study on ethyl-parathion removal from soil was performed employing PS activation using MW and proved the activation ability of the PS/MW system [14]. Besides, it was proven to be an effective method by using magnetic Fe_3O_4 as a PS activator under microwave irradiation to remove p-nitrophenol (PNP) in solution and also presented a potential application prospect in wastewater treatment [15]. In addition, compared to the MW-H_2O_2 system and ozonation process, the MW-PS system exhibited an excellent degradation result. For example, utilizing the MW/PS system to treat refractory organics in strongly alkaline dinitrodiazophenol wastewater, the removal rates of COD and chromaticity in 16 min were 74.07% and 99.40%, respectively [16]. Conclusively, the exceedingly good catalytic performance of MW is receiving increasing attention.

Recently, advanced oxidation processes (AOPs) have displayed the advantages of lower energy consumption, lower secondary pollution, and higher oxidation ability than traditional wastewater treatment technology. AOPs have attracted increasing attention due to their ability to generate reactive oxygen species (ROS, such as $SO_4\bullet^-$ and HO•) for oxidating or degrading refractory organic pollutants [17]. The method of generating HO• (E_0 = 2.8 V) and $SO_4\bullet^-$ (E_0 = 2.5–3.1 V) is activating persulfate (PS) using a series of methods, including heating, ultrasound, ultraviolet, and a transition metal oxide [18–22]. Transition metals, such as iron and cobalt, etc., have been utilized as chemical activation methods [20–22]. For instance, the Co_2FeAl-LDO/PMS system was used to degrade carbamazepine (CBZ). The results indicated that the system showed excellent degradation efficiency of CBZ (>99%) in 30 min, and the reaction rate constant was 0.2103 min^{-1} [23]. Besides, it is meaningful to study recalcitrant organic contaminants (ROCs) removal using cobalt ferrite $CoFe_2O_4$. This process achieved better destruction of four ROCs and offered a latent alternative method in water processing [24]. Therefore, a material with excellent PS activation and magnetic properties was developed and is presented in this study [17].

In this study, the application potential of $NiFe_2O_4$ was explored as a PS activator with the assistance of microwaves. The objective was to determine the function of ROSs during phenol degradation, explore the possible mechanism, and evaluate the safety of intermediate products.

2. Results and Discussion

2.1. Physicochemical Properties of $NiFe_2O_4$ Sample

The SEM technique was utilized to investigate the morphology of $NiFe_2O_4$, which is exhibited in Figure 2a. The SEM images showed that the catalyst $NiFe_2O_4$ had a uniform nanospherical structure, which coincided with previous studies.

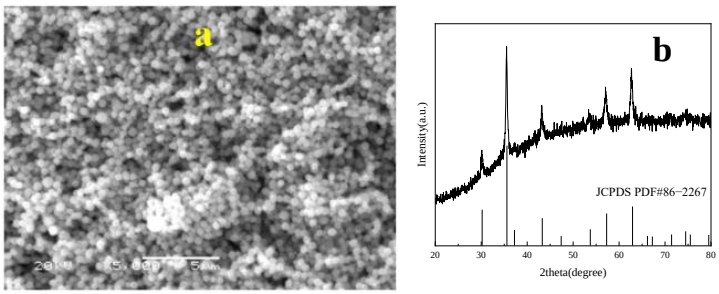

Figure 2. *Cont.*

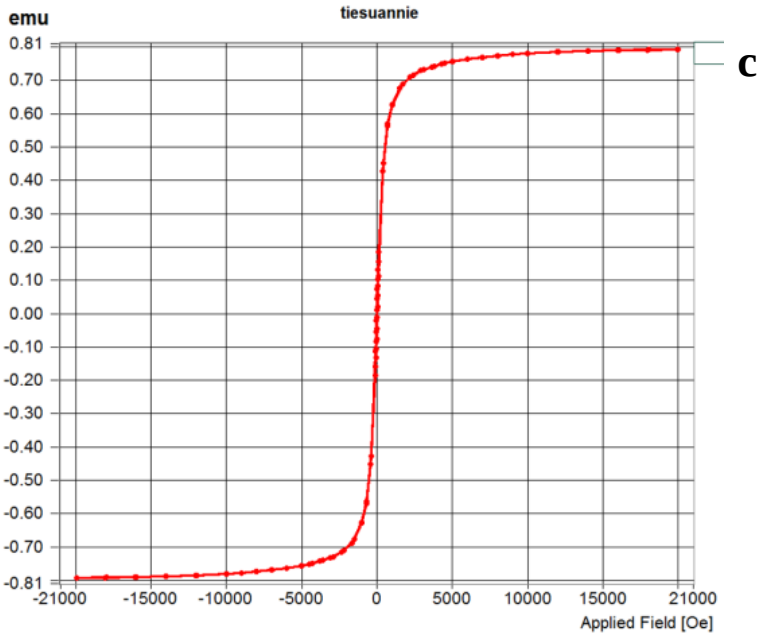

Figure 2. SEM image (**a**), XRD pattern (**b**), and VSM (**c**) of $NiFe_2O_4$.

The structure of the $NiFe_2O_4$ was determined by X-ray diffraction (XRD). As shown in Figure 2b, the diffraction peaks of $NiFe_2O_4$ appeared at 2θ = 18.4°, 30.3°, 35.7°, 43.4°, 53.8° 57.4°, and 62.9°, which corresponded to the Bragg planes of (220), (311), (222), (400), (422), (511), and (440), respectively. This is consistent with the standard based on their JCPDS cards, which proved that $NiFe_2O_4$ had been successfully fabricated [17,25,26].

Besides, the magnetic property of the $NiFe_2O_4$ sample was measured by a Vibrating Sample Magnetometer (VSM) at room temperature, and the results are exhibited in Figure 2c. The magnetization curve revealed a typical S-shape with the external magnetic field, indicating that $NiFe_2O_4$ is a ferromagnetic material [27]. It is of great significance for the recovery and reuse of the catalyst.

2.2. Phenol Degradation in the $NiFe_2O_4$ System

Batch control experiments were carried out to compare the phenol degradation ability of different reaction systems. As shown in Figure 3a, phenol using $NiFe_2O_4$, MW, and PS systems reached degradation rates of 6.84%, 35.78%, and 16.05% within 30 min, respectively. That is because $NiFe_2O_4$ possessed poor adsorption capacity for phenol, and it is difficult to exert the catalytic ability of pure PS effectively. For MW, based on previous studies, it has both thermal and non-thermal effects to remove phenol, so it shows a slightly stronger removal effect [10]. The treatment of phenol via using $NiFe_2O_4$/PS, systems reached degradation rates of, because PS only activated $SO_4\bullet^-$ and HO• on the surface of the catalyst [28]. However, in some combinatorial systems, such as MW+PS and MW+ $NiFe_2O_4$+PS, the removal effects of phenol were quite obvious, reaching 76.66% and 97.74% after a 30min reaction. In conclusion, relative to a single system ($NiFe_2O_4$, MW, and PS), the $NiFe_2O_4$ hybrid system had a more powerful ability to remove phenol. This could be explicated by the fact that $NiFe_2O_4$ and MW possess a synergy effect when they come together so they can display an excellent ability to activate PS for the degradation of phenol.

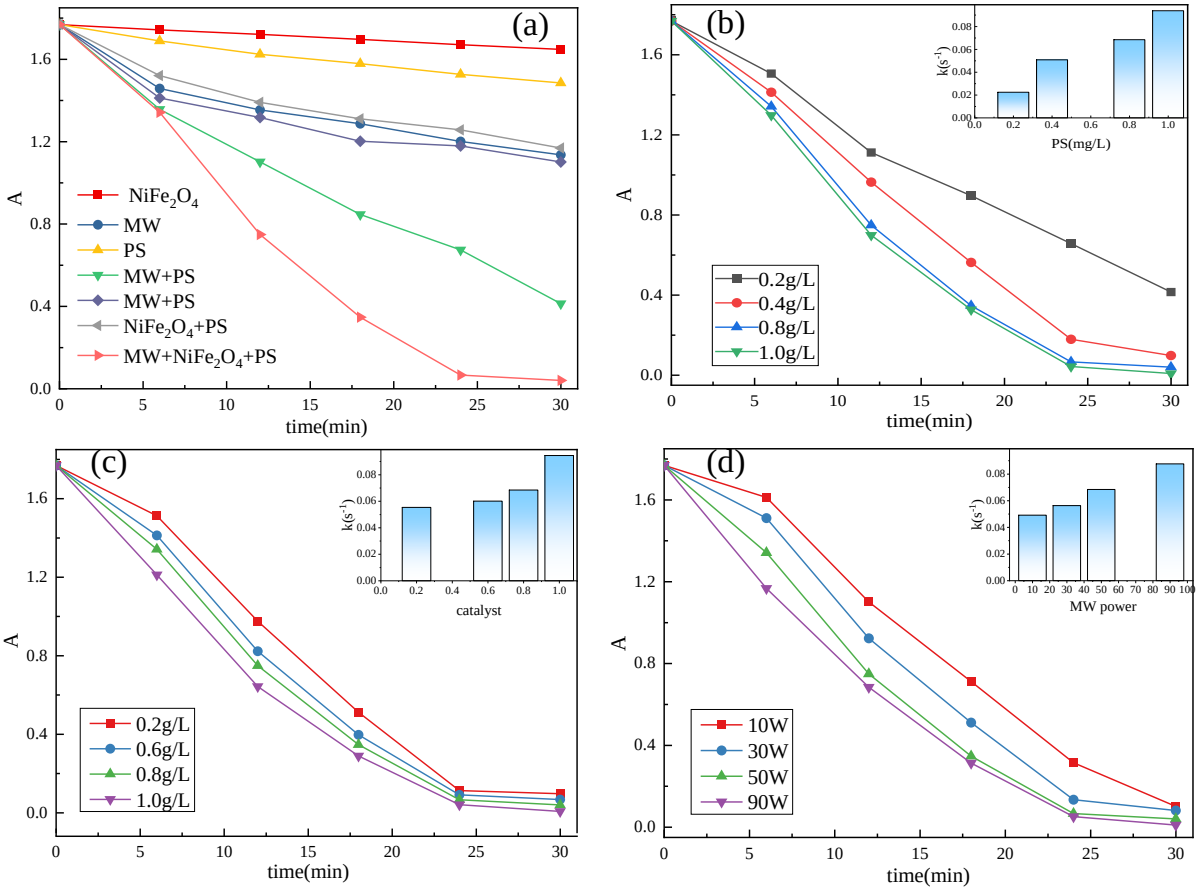

Figure 3. Degradation of phenol in solution under various reaction system (**a**), PS concentration (**b**), catalyst dosage (**c**), and MW power (**d**) (Reaction conditions: PS concentration = 0.4 g/L, catalyst dosage = 0.6 g/L, phenol concentration = 0.01 g/L, reaction temperature= 25 °C and initial pH value = 6.5 (unadjusted)).

2.3. Influences of Several Parameters on Phenol Degradation

2.3.1. Influence of PS Dosage

Figure 3b shows the relationship between the decomposition of phenol and PS dosages from 0.2 to 1 g/L. In the PS-catalytic process, the reactive radicals are related to the PS dosage [16]. As shown, the degradation rate of phenol was directly proportional to the dosage of PS. Specifically, when the PS dosage increased from 0.2 g/L to 0.8 g/L, the degradation growth rate of phenol increased from 76.5% to 97.7% within 30 min. The removal of phenol was obviously accelerated with the increasing PS concentration owing to the generation of more radicals [16]. Unfortunately, when the PS concentration continued to rise from 0.8 g/L to 1.0 g/L, the phenol degradation rate remained essentially constant (increased by 2%). The reaction rate increases with the increase in PS dosage. This phenomenon might be attributable to the fact that the high PS concentration could have a scavenger effect on SO4•⁻ as expressed in Equations (1) and (2) [6].

$$SO_4\bullet^- + SO_4\bullet^- \rightarrow S_2O_8^{2-} \quad (1)$$

$$SO_4\bullet^- + S_2O_8^{2-} \rightarrow S_2O_8\bullet^- + SO_4^{2-} \quad (2)$$

Thus, considering the economy and degradation efficiency, 0.4 g/L was considered to be the optimum PS concentration for later experiments.

2.3.2. Influence of $NiFe_2O_4$ Dosage

It is widely known that the dosage of the catalyst is vital for the removal experiment of pollutants in the PS system. Consequently, a series of tests were carried out to examine the effect of the $NiFe_2O_4$ dosage with no variation of other factors. As Figure 3c illustrated, the removal efficiency of phenol increased with the growth of the $NiFe_2O_4$ dosage in the experiments. The reaction rate increases with the increase in $NiFe_2O_4$ dosage. That may be due to the fact that when the catalyst concentration increased, the active sites, which were used to activate PS in the reaction system, were correspondingly added [29,30]. So, taking into account the cost of the $NiFe_2O_4$/PS system, 0.6 g/L seemed to be the optimum catalyst concentration.

2.3.3. Influence of the MW Power

In the $NiFe_2O_4$ system, based on previous research, the power of MW also plays an important role in phenol degradation [15]. So, the influence of microwaves was also discussed in this study, and the results are exhibited in Figure 3d. As we can see, when the power of MW increased (10 W, 30 W, 50 W, and 90 W), the phenol degradation rate also increased (94.3%, 95.4%, 97.7%, and 99.4% within 30 min) and the reaction rate increased with the increase in MW power. This could be explained by the fact that (i) the reaction system could be heated by the MW and led to the system temperature increasing, which could accelerate the phenol degradation reaction. (ii) Previous research also proved that MW could accelerate the dispersion and mass transfer of catalysts [15]. (iii) In the system, the synergetic effect between the MW and PS occurred for phenol degradation, which was strengthened as the MW power increased [12,15].

2.3.4. Roles of the Initial pH in Phenol Degradation

In fact, the initial pH of practical water is diverse in different environments and plays a crucial role in the production and behavior of free radicals [31]. So, it has an important sense to explore the impact of the initial system pH in degradation experiments. As observed from Figure 4a, after a 30 min reaction, more than 95% phenol could be removed in all the initial pH situations (pH = 2, 4, 6, 8,m and 10). Noticeably, when the system's initial pH rose to 6, the degradation rate speeded up markedly. The rate constant reached the maximum of 0.06844 s^{-1}. That indicated the $NiFe_2O_4$ system had a wide range of pH adaptability. The majority of natural water has a pH range of 5-9 [32], so the $NiFe_2O_4$ system would be of great significance in practical applications.

2.3.5. Influence of the Co-Existing Anions

The ion condition in natural water is very complex. So, for the sake of the practicability of the system, some common and abundant anions in natural water were appended to the simulated sewage (such as Cl^-, $H_2PO_4^-$, HCO_3^-, NO_3^-, and HA). As shown in Figure 4b, Cl^-, $H_2PO_4^-$, HCO_3^-, and NO_3^- played a negative role in the reaction, and the inhibitory effects were $H_2PO_4^-$ (5.99%) > HCO_3^- (19.95%) > NO_3^- (66.02%) > Cl^- (91.29%) after the 30 minute reaction. On the contrary, the degradation of phenol was enhanced, and the removal efficiency achieved 99.94% with the presence of HA. This phenomenon could be explained by the fact that anions could react with $SO_4\bullet^-$ in the system and this would cause a negative effect on phenol decomposition. Moreover, as a kind of natural organic matter, HA is rich in water and its active sites could promote the generation of $SO_4\bullet^-$ from PS. The corresponding reactions are listed below (Equations (3)–(11)) [17,23,33–37]:

$$SO_4\bullet^- + Cl^- \rightarrow SO_4^{2-} + Cl\bullet \quad (3)$$

$$Cl\bullet + Cl^- \rightarrow Cl_2\bullet^- \quad (4)$$

$$\bullet OH + Cl^- \rightarrow ClOH\bullet^- \quad (5)$$

$$SO_4\bullet^- + HCO_3^- \rightarrow SO_4^{2-} + HCO_3\bullet \quad (6)$$

$$NO_3^- + SO_4\bullet^- \rightarrow NO_3\bullet + SO_4^{2-} \quad (7)$$

$$NO_3^- + \bullet OH \rightarrow OH^- + \bullet NO_2 \quad (8)$$

$$H_2PO_4^- + SO_4\bullet^- \rightarrow H_2PO_4\bullet + SO_4^{2-} \quad (9)$$

$$HCO_3^- + SO_4\bullet^- \rightarrow SO_4^{2-} + CO_3\bullet^- + H^+ \quad (10)$$

$$HCO_3^- + \bullet OH \rightarrow CO_3\bullet^- + H_2O \quad (11)$$

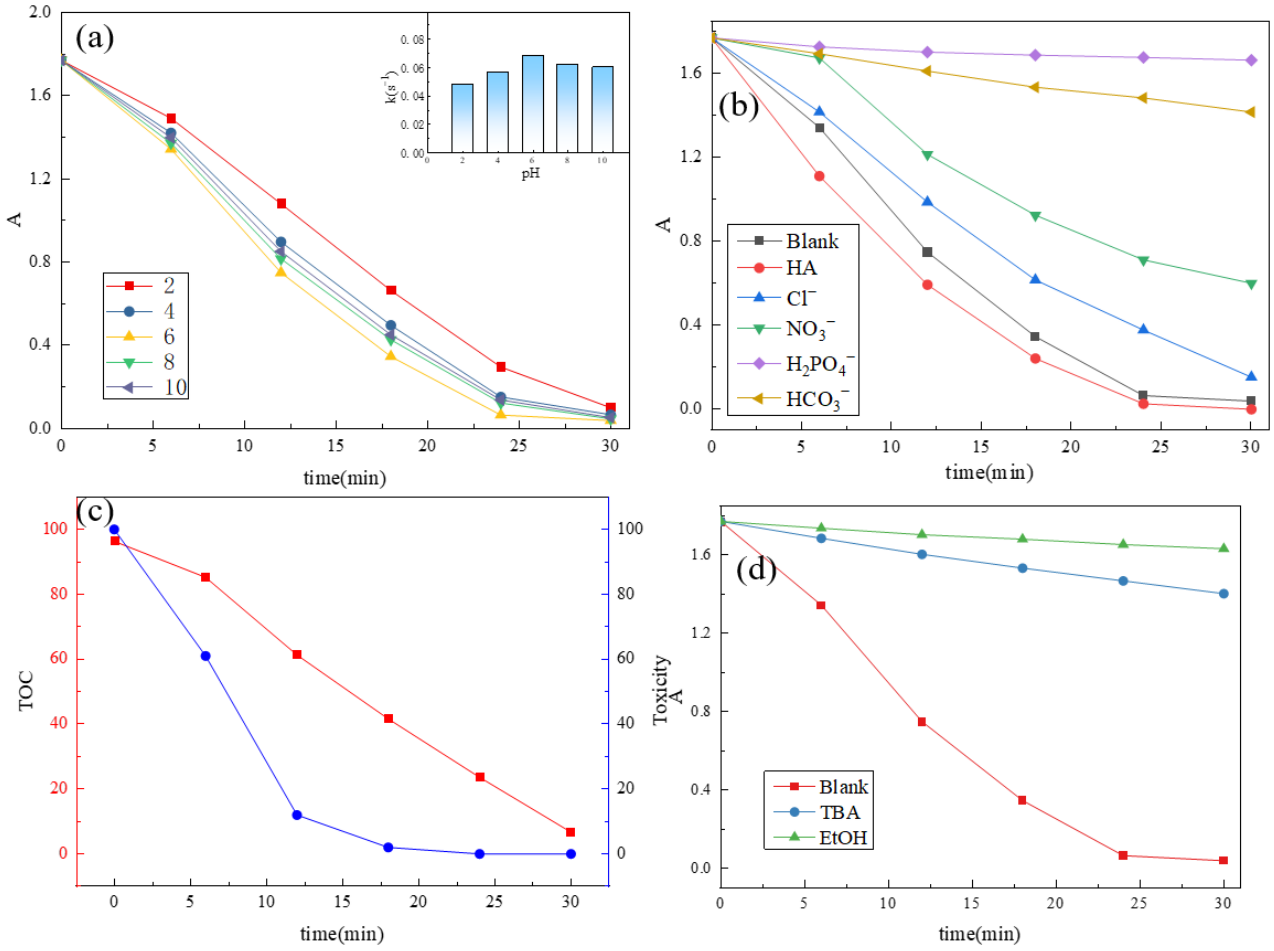

Figure 4. Different reactions' initial pH in the system of $NiFe_2O_4$ (**a**), the co-existing anions (**b**), TOC and toxicity analysis (**c**), and different inhibition experiments (**d**) (Reaction conditions: PS concentration = 0.4 g/L, catalyst dosage = 0.6 g/L, phenol concentration = 0.01 g/L, inhibition dosage = 50 mmol, reaction temperature = 25 °C and initial pH value = 6.5 (unadjusted)).

2.4. Mineralization Ability and Toxicity Analysis

TOC is often utilized to detect the degree of contaminant mineralization in the catalytic reaction [2]. In this study, a change in phenol TOC was also observed, and the results are exhibited in Figure 4c. It was clear that the TOC degradation efficiency increased slowly over the period of 30 min, and a 93.04% mineralization efficiency was reached for phenol after the reaction in the $NiFe_2O_4$ system. In addition, in the whole reaction process, the toxicity of the system was reduced, which indicated that the toxicity of the decomposition intermediates had decreased [12,13]. All the analyses and results proved that the $NiFe_2O_4$ system could effectively reduce the toxic intermediates during the degradation of the LVF solution.

2.5. Mechanism Analysis

In order to explore the PS activation mechanism in the $NiFe_2O_4$ system, radical inhibition tests were carried out to detect the function of HO• and SO_4•$^-$ in the degradation of phenol. As is well known, ethanol (EtOH) and tertiary butanol (TBA) are considered common inhibitors in experiments [13,38–41]. The reaction constant between TBA and HO• is (4–9.1) $\times 10^5$ M^{-1}•s^{-1} and that between TBA and SO_4•$^-$ is (3.8–7.6) $\times$ 10^8 M^{-1}•s^{-1}. There is a big difference between the two reaction constants, so TBA is utilized as a scavenger for HO•. EtOH can quickly react with both SO_4•$^-$ ((1.6–7.7) $\times 10^7$ M^{-1}•s^{-1}) and HO• ((1.2–2.8) $\times 10^9$ M^{-1}•s^{-1}). As seen in Figure 4d, the phenol degradation efficiency was 97.74% in the non-inhibitor system within 30 min; however, it dropped to 20.8% and 7.86%, respectively, after the participation of TBA and EtOH. The results meant that both the decomposition rate of phenol was reduced after the addition of EtOH and TBA and the inhibition influence was higher in the EtOH-PMS system. To summarize, both HO• and SO_4•$^-$ participated in the reaction, and SO_4•$^-$ played a larger role in the decomposition reaction system.

Based on the above discussion and results, the mechanism of enhanced PS activation with the $NiFe_2O_4$/MW was proposed and exhibited in Figure 5. The addition of $NiFe_2O_4$, Fe^{3+}, and Ni^{2+}, which acted as activation centers on the catalyst surface, activated PS to generate SO_4•$^-$. SO_4•$^-$mainly performed electronic transfer and HO• played the role of addition and hydrogen absorption [16]. Furthermore, Fe^{3+} was able to become Fe^{2+} when the system was in the presence of Ni^{2+}. In addition, the existence of MW could boost the above reaction [37,42,43]. The thorough oxidation reactions are displayed below:

$$Ni^{2+} + S_2O_8^{2-} \rightarrow Ni^{3+} + SO_4\bullet^- + SO_4^{2-} \quad (12)$$

$$Ni^{2+} + Fe^{3+} \rightarrow Ni^{3+} + Fe^{2+} \quad (13)$$

$$Fe^{2+} + S_2O_8^{2-} \rightarrow Fe^{3+} + SO_4\bullet^- + SO_4^{2-} \quad (14)$$

$$2H_2O + S_2O_8^{2-} \rightarrow HSO_5^- + HSO_4^- \quad (15)$$

$$Ni^{3+} + HSO_5^- \rightarrow Ni^{2+} + SO_5\bullet^- + H^+ \quad (16)$$

$$SO_4\bullet^- + H_2O \rightarrow SO_4^{2-} + 3H^+ + HO\bullet \quad (17)$$

$$SO_4\bullet^- + OH^- \rightarrow SO_4^{2-} + HO\bullet \quad (18)$$

$$Phenol + SO_4\bullet^- + HO\bullet \rightarrow products \quad (19)$$

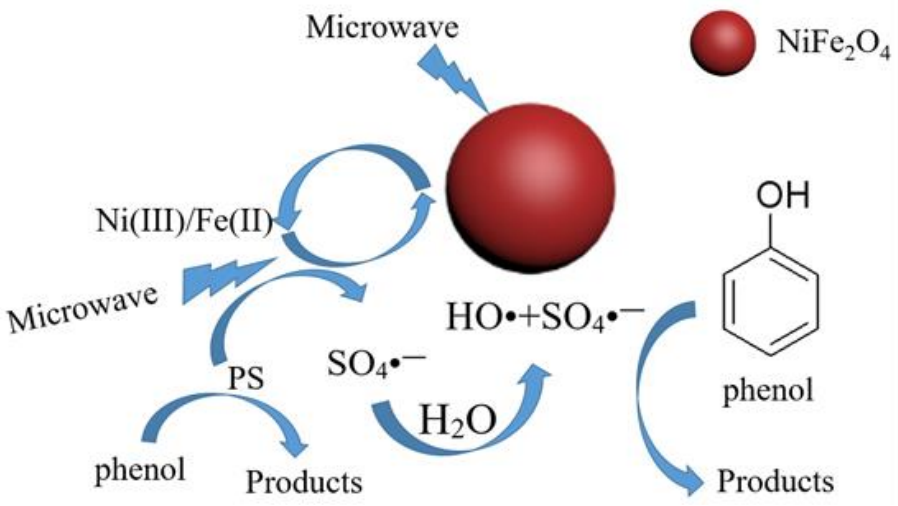

Figure 5. Proposed mechanism of $NiFe_2O_4$ system for phenol degradation.

2.6. Stability of $NiFe_2O_4$

In addition, as an important concern for potential applications, the catalytic stability of the catalyst was estimated through consecutive repeated degradation reactions in identical experimental conditions utilizing recycled material, and the results are displayed in Figure 6. Compared with the fresh catalyst, the removal of phenol in 30 min was able to reach 96% after the eighth run. Compared with the first time, there was almost no change in the amount of phenol removal the second time. In the third to eighth trials, a slight decrease in the removal of phenol was observed. Obviously, the $NiFe_2O_4$ system exhibited excellent degradation performance and stability on the whole. Therefore, according to these outcomes and the XRD atlases, we could come to the conclusion that the prepared $NiFe_2O_4$ catalytic material possessed outstanding structure and catalytic stability, so it is a promising catalyst. The thermal analysis (Figure 7) shows that there is no weight change in the temperature range of 0–1000 °C, which proves the stability of the material.

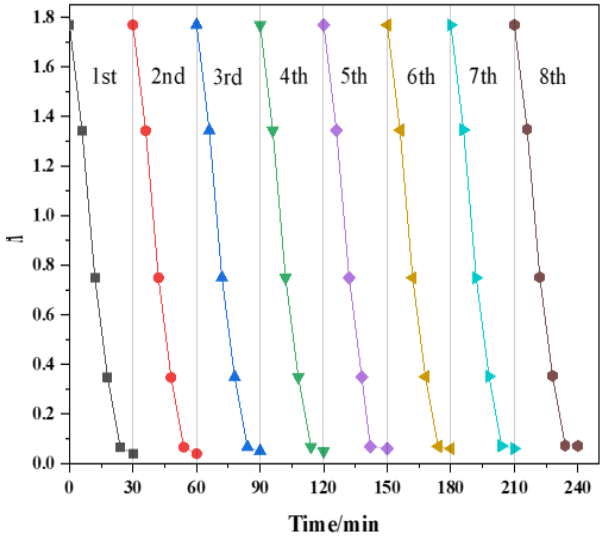

Figure 6. Reusability experiments of the $NiFe_2O_4$ system (Reaction conditions: PS concentration = 0.4 g/L, catalyst dosage = 0.6 g/L, reaction temperature = 25 °C, phenol concentration = 0.01 g/L and initial pH value = 6.5 (unadjusted)).

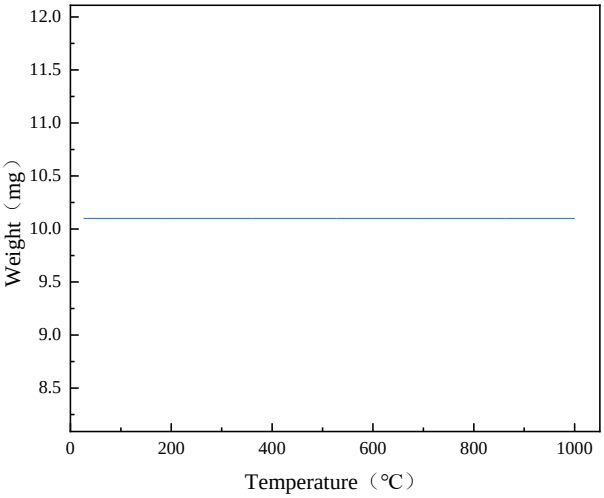

Figure 7. TGA curves of the $NiFe_2O_4$.

3. Experiments

3.1. Chemicals

Iron chloride ($FeCl_3 \cdot 6H_2O$), nickel chloride ($NiCl_2 \cdot 6H_2O$), ferrous chloride ($FeCl_2 \cdot 4H_2O$), ethylene glycol ($C_2H_6O_2$), sodium chloride (NaCl), sodium bicarbonate ($NaHCO_3$), sodium nitrate ($NaNO_3$), sodium dihydrogen phosphate (NaH_2PO_4), phenol (C_6H_5OH), potassium persulfate (PS), and absolute ethanol (C_2H_5OH) were purchased from Kermel Chemical Reagent Co., Ltd., (Tianjin, China). Tert-Butanol ($C_4H_{10}O$ (TBA)) was obtained from Sinopharm Chemical Reagent Co., Ltd., (Shanghai, China). In addition, phenol was provided by Aladdin Chemistry Co., Ltd., (Shanghai, China). All the chemicals were of analytical grade and used without further purification. Deionized water (DI) was used throughout this experiment.

3.2. Synthesis of $NiFe_2O_4$ Sample

In this study, Nickel ferrite ($NiFe_2O_4$) was synthesized according to a previous study. In detail, 1.63 g $FeCl_3 \cdot 6H_2O$ and 0.72 g $NiCl_2 \cdot 6H_2O$ were dissolved in a 60 mL ethylene solution and sonicated for half an hour. Afterwards, the mixture was transferred to a 100 mL Teflon-lined stainless-steel autoclave, sealed, and heated at 200 °C for 12 h. At given time intervals, the autoclave was cooled to room temperature and then filtered. Subsequently, the obtained samples were washed by DI and EtOH repeatedly (four times in this case). Eventually, $NiFe_2O_4$ was dried at 60 °C for 3 h.

3.3. Characterizations

The morphology and elemental analysis of $NiFe_2O_4$ were detected by SEM (Japan Electron Optics Laboratory Co., Ltd., Tokyo, Japan). The XRD patterns of the catalyst were obtained on a D/Max-2004 X-ray powder diffractometer (Bruker, Germany) with Cu Kα radiation (λ = 0.15426 nm). Besides, the magnetic properties of the $NiFe_2O_4$ samples were measured by VSM (Lake Shore 7303) at 26 °C.

3.4. Degradation of Phenol Solution

In this study, phenol degradation experiments were conducted in 150 mL conical flasks, in which a certain amount of the sample and PMS were placed into the flasks, which had a 50 mL 10 mg/L phenol solution to start the degradation reaction. Then, they were placed in a microwave instrument with a certain power. After a certain intermission, 5 mL of the sample was collected from the reaction solution and filtered through a 0.22 μm filter. Finally, the concentration of phenol was measured using the colorimetric method of 4-aminoantipyrine at the characteristic wavelength of 510 nm [3]. It should be noted that the mineralization ability and toxicity analysis were evaluated by a TOC analyzer and activated sludge process, respectively. Finally, the major reaction factors of phenol degradation were also discussed. In particular, the complete degradation was conducted in duplicate to reduce errors.

4. Conclusions

To summarize, the $NiFe_2O_4$ system was excellent in the degradation of phenol. In this process, several methods (XRD, SEM, and VSM) were carried out to characterize $NiFe_2O_4$. Then, phenol removal tests were conducted in different situations with the $NiFe_2O_4$ system to evaluate the activation properties of this system. The results were as follows: (i) A series of characterization detections proved that $NiFe_2O_4$ was successfully synthesized. (ii) Multiple sets of experiments proved that the $NiFe_2O_4$ system possessed excellent removal effectiveness for phenol, and achieved a removal efficiency of 97.74% within 30 min. Besides, the ideal degradation conditions were also found, regarding the PS dosage (0.4 g/L), $NiFe_2O_4$ concentration (0.6 g/L), and MW power (50 W). Moreover, the $NiFe_2O_4$ system had good adaptability across a wide range of pH values. The quenching experiment confirmed both the HO• and $SO_4\bullet^-$ played a vital role in the experiments, and $H_2PO_4^-$, HCO_3^-, NO_3^-, and Cl^- could hinder the reaction process but NOM could

promote it. (iii) Through the mineralization ability and toxicity analysis, phenol was proven to be almost completely mineralized, and the toxicity was greatly reduced by the $NiFe_2O_4$ system. Reusability and stability experiments confirmed the excellent stability and cyclicity of the $NiFe_2O_4$ catalyst. (iiii) In particular, based on the results of the experiments, the possible mechanism of phenol degradation was proposed.

Author Contributions: Conceptualization, Y.L.; methodology, Y.L.; software, W.L.; validation, Y.L., W.L. and S.J.; formal analysis, W.L.; investigation, S.J.; resources, W.L.; data curation, Y.L.; writing—original draft preparation, Y.L.; writing—review and editing, X.C. and L.L.; visualization, S.J.; supervision, S.J.; project administration, X.C. and L.L.; funding acquisition, X.C. and L.L. All authors have read and agreed to the published version of the manuscript.

Funding: This research was funded by [the Natural Science Foundation of Gansu Province] grant number [21JR1RA239].

Conflicts of Interest: The authors declare no conflict of interest.

References

1. Wu, H.; Xu, X.; Shi, L.; Yin, Y.; Zhang, L.-C.; Wu, Z.; Duan, X.; Wang, S.; Sun, H. Manganese Oxide Integrated Catalytic Ceramic Membrane for Degradation of Organic Pollutants Using Sulfate Radicals. *Water Res.* **2019**, *167*, 115110. [CrossRef] [PubMed]
2. Li, M.; Huang, F.; Hu, L.; Sun, W.; Li, E.; Xiong, D.; Zhong, H.; He, Z. Efficient Activation of Peroxymonosulfate by a Novel Catalyst Prepared Directly from Electrolytic Manganese Slag for Degradation of Recalcitrant Organic Pollutes. *Chem. Eng. J.* **2020**, *401*, 126085. [CrossRef]
3. Othman, I.; Hisham Zain, J.; Abu Haija, M.; Banat, F. Catalytic Activation of Peroxymonosulfate Using $CeVO_4$ for Phenol Degradation: An Insight into the Reaction Pathway. *Appl. Catal. B Environ.* **2020**, *266*, 118601. [CrossRef]
4. Qin, F.-X.; Jia, S.-Y.; Liu, Y.; Han, X.; Ren, H.-T.; Zhang, W.-W.; Hou, J.-W.; Wu, S.-H. Metal-Organic Framework as a Template for Synthesis of Magnetic $CoFe_2O_4$ Nanocomposites for Phenol Degradation. *Mater. Lett.* **2013**, *101*, 93–95. [CrossRef]
5. Wu, M.; Ouyang, Y.; Zhao, K.; Ma, Y.; Wang, M.; Liu, D.; Su, Y.; Jin, P. A Novel Fabrication Method for Titanium Dioxide/Activated Carbon Fiber Electrodes and the Effects of Titanium Dioxide on Phenol Degradation. *J. Environ. Chem. Eng.* **2016**, *4*, 3646–3653. [CrossRef]
6. Liu, X.; Liu, Y.; Lu, S.; Wang, Z.; Wang, Y.; Zhang, G.; Guo, X.; Guo, W.; Zhang, T.; Xi, B. Degradation Difference of Ofloxacin and Levofloxacin by UV/H_2O_2 and UV/PS (Persulfate): Efficiency, Factors and Mechanism. *Chem. Eng. J.* **2020**, *385*, 123987. [CrossRef]
7. Sun, T.; Gu, B.; Wang, X.; Wang, Y.; Long, Y.; Fan, G. The Simplest and Ultrafast Microwave-Mediated Solid-State Construction of Cobalt Oxide/Carbon Hybrid as an Efficient Peroxymonosulfate Activator for Ciprofloxacin Degradation. *Sep. Purif. Technol.* **2022**, *296*, 121346. [CrossRef]
8. Kan, H.; Wang, T.; Yu, J.; Qu, G.; Zhang, P.; Jia, H.; Sun, H. Remediation of Organophosphorus Pesticide Polluted Soil Using Persulfate Oxidation Activated by Microwave. *J. Hazard. Mater.* **2021**, *401*, 123361. [CrossRef]
9. Qi, C.; Liu, X.; Lin, C.; Zhang, X.; Ma, J.; Tan, H.; Ye, W. Degradation of Sulfamethoxazole by Microwave-Activated Persulfate: Kinetics, Mechanism and Acute Toxicity. *Chem. Eng. J.* **2014**, *249*, 6–14. [CrossRef]
10. Hu, L.; Wang, P.; Zhang, G.; Liu, G.; Li, Y.; Shen, T.; Crittenden, J.C. Enhanced Persulfate Oxidation of Organic Pollutants and Removal of Total Organic Carbons Using Natural Magnetite and Microwave Irradiation. *Chem. Eng. J.* **2020**, *383*, 123140. [CrossRef]
11. Peng, J.; Wang, Z.; Wang, S.; Liu, J.; Zhang, Y.; Wang, B.; Gong, Z.; Wang, M.; Dong, H.; Shi, J.; et al. Enhanced Removal of Methylparaben Mediated by Cobalt/Carbon Nanotubes (Co/CNTs) Activated Peroxymonosulfate in Chloride-Containing Water: Reaction Kinetics, Mechanisms and Pathways. *Chem. Eng. J.* **2021**, *409*, 128176. [CrossRef]
12. Gao, Y.; Zou, D. Efficient Degradation of Levofloxacin by a Microwave–3D $ZnCo_2O_4$/Activated Persulfate Process: Effects, Degradation Intermediates, and Acute Toxicity. *Chem. Eng. J.* **2020**, *393*, 124795. [CrossRef]
13. Zhang, H.; Wang, J.; Zhang, X.; Li, B.; Cheng, X. Enhanced Removal of Lomefloxacin Based on Peroxymonosulfate Activation by Co_3O_4/δ-FeOOH Composite. *Chem. Eng. J.* **2019**, *369*, 834–844. [CrossRef]
14. Miao, D.; Zhao, S.; Zhu, K.; Zhang, P.; Wang, T.; Jia, H.; Sun, H. Activation of Persulfate and Removal of Ethyl-Parathion from Soil: Effect of Microwave Irradiation. *Chemosphere* **2020**, *253*, 126679. [CrossRef] [PubMed]
15. Hu, L.; Wang, P.; Liu, G.; Zheng, Q.; Zhang, G. Catalytic Degradation of P-Nitrophenol by Magnetically Recoverable Fe_3O_4 as a Persulfate Activator under Microwave Irradiation. *Chemosphere* **2020**, *240*, 124977. [CrossRef] [PubMed]
16. Wan, Y.; Wan, J.; Zhao, J.R.; Wang, Y.; Luo, T.; Yang, S.; Liu, Y. Facile Preparation of Iron Oxide Doped Fe-MOFs-MW as Robust Peroxydisulfate Catalyst for Emerging Pollutants Degradation. *Chemosphere* **2020**, *254*, 126798. [CrossRef]
17. Wang, Z.; Zhang, X.; Zhang, H.; Zhu, G.; Gao, Y.; Cheng, Q.; Cheng, X. Synthesis of Magnetic Nickel Ferrite/Carbon Sphere Composite for Levofloxacin Elimination by Activation of Persulfate. *Sep. Purif. Technol.* **2019**, *215*, 528–539. [CrossRef]

18. Wang, S.; Wang, J. Oxidative Removal of Carbamazepine by Peroxymonosulfate (PMS) Combined to Ionizing Radiation: Degradation, Mineralization and Biological Toxicity. *Sci. Total Environ.* **2019**, *658*, 1367–1374. [CrossRef]
19. Ding, Y.; Zhu, L.; Wang, N.; Tang, H. Sulfate Radicals Induced Degradation of Tetrabromobisphenol A with Nanoscaled Magnetic $CuFe_2O_4$ as a Heterogeneous Catalyst of Peroxymonosulfate. *Appl. Catal. B Environ.* **2013**, *129*, 153–162. [CrossRef]
20. Devi, P.; Das, U.; Dalai, A.K. In-Situ Chemical Oxidation: Principle and Applications of Peroxide and Persulfate Treatments in Wastewater Systems. *Sci. Total Environ.* **2016**, *571*, 643–657. [CrossRef]
21. Wacławek, S.; Lutze, H.V.; Grübel, K.; Padil, V.V.T.; Černík, M.; Dionysiou, D.D. Chemistry of Persulfates in Water and Wastewater Treatment: A Review. *Chem. Eng. J.* **2017**, *330*, 44–62. [CrossRef]
22. Wang, J.; Wang, S. Activation of Persulfate (PS) and Peroxymonosulfate (PMS) and Application for the Degradation of Emerging Contaminants. *Chem. Eng. J.* **2018**, *334*, 1502–1517. [CrossRef]
23. Sun, Q.-T.; Xu, B.-D.; Yang, J.; Qian, T.-T.; Jiang, H. Layered Oxides Supported Co-Fe Bimetal Catalyst for Carbamazepine Degradation via the Catalytic Activation of Peroxymonosulfate. *Chem. Eng. J.* **2020**, *400*, 125899. [CrossRef]
24. Cai, C.; Kang, S.; Xie, X.; Liao, C.; Duan, X.; Dionysiou, D.D. Efficient Degradation of Bisphenol A in Water by Heterogeneous Activation of Peroxymonosulfate Using Highly Active Cobalt Ferrite Nanoparticles. *J. Hazard. Mater.* **2020**, *399*, 122979. [CrossRef]
25. Zeynizadeh, B.; Rahmani, S.; Eghbali, E. Anchored Sulfonic Acid on Silica-Layered $NiFe_2O_4$: A Magnetically Reusable Nanocatalyst for Hantzsch Synthesis of 1,4-Dihydropyridines. *Polyhedron* **2019**, *168*, 57–66. [CrossRef]
26. Chen, Y.; Li, M.; Tong, Y.; Liu, Z.; Fang, L.; Wu, Y.; Fang, Z.; Wu, F.; Huang, L.-Z. Radical Generation via Sulfite Activation on $NiFe_2O_4$ Surface for Estriol Removal: Performance and Mechanistic Studies. *Chem. Eng. J.* **2019**, *368*, 495–503. [CrossRef]
27. Abroshan, E.; Farhadi, S.; Zabardasti, A. Novel Magnetically Separable $Ag_3PO_4/MnFe_2O_4$ Nanocomposite and Its High Photocatalytic Degradation Performance for Organic Dyes under Solar-Light Irradiation. *Sol. Energy Mater. Sol. Cells* **2018**, *178*, 154–163. [CrossRef]
28. Tong, X.; Ma, S.; Qi, Y.; Li, J.; Yao, T.; Wu, J. Synthesis of FeCo Alloy Encapsulated Nitrogen-Doped Graphitized Carbon: High Catalytic Activation and Low Metal Ion Leaching in Microwave Assisted Fenton Reaction. *J. Taiwan Inst. Chem. Eng.* **2020**, *108*, 64–70. [CrossRef]
29. Ma, Q.; Zhang, H.; Zhang, X.; Li, B.; Guo, R.; Cheng, Q.; Cheng, X. Synthesis of Magnetic $CuO/MnFe_2O_4$ Nanocompisite and Its High Activity for Degradation of Levofloxacin by Activation of Persulfate. *Chem. Eng. J.* **2019**, *360*, 848–860. [CrossRef]
30. Lai, L.; Yan, J.; Li, J.; Lai, B. Co/Al_2O_3-EPM as Peroxymonosulfate Activator for Sulfamethoxazole Removal: Performance, Biotoxicity, Degradation Pathways and Mechanism. *Chem. Eng. J.* **2018**, *343*, 676–688. [CrossRef]
31. Guo, R.; Wang, Y.; Li, J.; Cheng, X.; Dionysiou, D.D. Sulfamethoxazole Degradation by Visible Light Assisted Peroxymonosulfate Process Based on Nanohybrid Manganese Dioxide Incorporating Ferric Oxide. *Appl. Catal. B Environ.* **2020**, *278*, 119297. [CrossRef]
32. Yin, R.; Guo, W.; Wang, H.; Du, J.; Zhou, X.; Wu, Q.; Zheng, H.; Chang, J.; Ren, N. Enhanced Peroxymonosulfate Activation for Sulfamethazine Degradation by Ultrasound Irradiation: Performances and Mechanisms. *Chem. Eng. J.* **2018**, *335*, 145–153. [CrossRef]
33. Ji, Y.; Dong, C.; Kong, D.; Lu, J. New Insights into Atrazine Degradation by Cobalt Catalyzed Peroxymonosulfate Oxidation: Kinetics, Reaction Products and Transformation Mechanisms. *J. Hazard. Mater.* **2015**, *285*, 491–500. [CrossRef] [PubMed]
34. Deng, J.; Xu, M.; Feng, S.; Qiu, C.; Li, X.; Li, J. Iron-Doped Ordered Mesoporous Co3O4 Activation of Peroxymonosulfate for Ciprofloxacin Degradation: Performance, Mechanism and Degradation Pathway. *Sci. Total Environ.* **2019**, *658*, 343–356. [CrossRef]
35. Nie, M.; Deng, Y.; Nie, S.; Yan, C.; Ding, M.; Dong, W.; Dai, Y.; Zhang, Y. Simultaneous Removal of Bisphenol A and Phosphate from Water by Peroxymonosulfate Combined with Calcium Hydroxide. *Chem. Eng. J.* **2019**, *369*, 35–45. [CrossRef]
36. Ahmadi, M.; Ghanbari, F. Organic Dye Degradation through Peroxymonosulfate Catalyzed by Reusable Graphite Felt/Ferriferrous Oxide: Mechanism and Identification of Intermediates. *Mater. Res. Bull.* **2019**, *111*, 43–52. [CrossRef]
37. Duan, X.; Sun, H.; Kang, J.; Wang, Y.; Indrawirawan, S.; Wang, S. Insights into Heterogeneous Catalysis of Persulfate Activation on Dimensional-Structured Nanocarbons. *Acs Catal.* **2015**, *5*, 4629–4636. [CrossRef]
38. Zhou, Y.; Jiang, J.; Gao, Y.; Ma, J.; Pang, S.-Y.; Li, J.; Lu, X.-T.; Yuan, L.-P. Activation of Peroxymonosulfate by Benzoquinone: A Novel Nonradical Oxidation Process. *Environ. Sci. Technol.* **2015**, *49*, 12941–12950. [CrossRef]
39. Li, C.-X.; Chen, C.-B.; Lu, J.-Y.; Cui, S.; Li, J.; Liu, H.-Q.; Li, W.-W.; Zhang, F. Metal Organic Framework-Derived $CoMn_2O_4$ Catalyst for Heterogeneous Activation of Peroxymonosulfate and Sulfanilamide Degradation. *Chem. Eng. J.* **2018**, *337*, 101–109. [CrossRef]
40. Abdul Nasir Khan, M.; Kwame Klu, P.; Wang, C.; Zhang, W.; Luo, R.; Zhang, M.; Qi, J.; Sun, X.; Wang, L.; Li, J. Metal-Organic Framework-Derived Hollow Co_3O_4/Carbon as Efficient Catalyst for Peroxymonosulfate Activation. *Chem. Eng. J.* **2019**, *363*, 234–246. [CrossRef]
41. Zhang, J.; Shao, X.; Shi, C.; Yang, S. Decolorization of Acid Orange 7 with Peroxymonosulfate Oxidation Catalyzed by Granular Activated Carbon. *Chem. Eng. J.* **2013**, *232*, 259–265. [CrossRef]
42. Liu, F.; Zhou, H.; Pan, Z.; Liu, Y.; Yao, G.; Guo, Y.; Lai, B. Degradation of Sulfamethoxazole by Cobalt-Nickel Powder Composite Catalyst Coupled with Peroxymonosulfate: Performance, Degradation Pathways and Mechanistic Consideration. *J. Hazard. Mater.* **2020**, *400*, 123322. [CrossRef] [PubMed]
43. Guan, R.; Yuan, X.; Wu, Z.; Wang, H.; Jiang, L.; Zhang, J.; Li, Y.; Zeng, G.; Mo, D. Accelerated Tetracycline Degradation by Persulfate Activated with Heterogeneous Magnetic $Ni_xFe_{3-x}O_4$ Catalysts. *Chem. Eng. J.* **2018**, *350*, 573–584. [CrossRef]